Appl. Phys. A 78, 231–238 (2004)
DOI: 10.1007/s00339-003-2307-1

Applied Physics A
Materials Science & Processing

C. BACH[1]
T. KLÜNER[2]
A. GROSS[1,✉]

Multi-dimensional mixed quantum–classical description of the laser-induced desorption of molecules

[1] Physik-Department T30, Technische Universität München, 85747 Garching, Germany
[2] Fritz-Haber-Institut, Faradayweg 4–6, 14195 Berlin, Germany

Received: 30 April 2003/Accepted: 4 July 2003
Published online: 31 October 2003 •

ABSTRACT A mixed quantum–classical method for the simulation of laser-induced desorption processes at surfaces is implemented. In this method, the nuclear motion is described classically, while the electrons are treated quantum mechanically. The feedback between nuclei and electrons is taken into account self-consistently. The computational efficiency of this method allows a more realistic multi-dimensional treatment of desorption processes. We apply this method to the laser-induced desorption of NO from NiO(100) using a two-state two-dimensional potential energy surface derived from ab initio quantum chemical calculations; we extend this potential energy surface to seven dimensions employing a physically reasonable model potential. By comparing our method to jumping wave-packet calculations on exactly the same potential energy surface we verify the validity of our method. We focus on the velocity, rotational, and vibrational distributions of the desorbing NO molecules. Furthermore, we model the energy transfer to the substrate by a surface oscillator. Including recoil processes in the simulation has a decisive influence on the desorption dynamics, as far as the velocity and rotational distribution is concerned. In particular, the bimodality in the velocity distribution observed in low dimensions and in the experiment disappears in a high-dimensional treatment.

PACS 68.43.Tj; 68.43.Rs; 82.20.Gk; 82.20.Wt

1 Introduction

Photon- and electron-stimulated desorption of molecules from surfaces has been intensively studied in the last decades [1]. In both kinds of processes, the desorption is induced by electronic transitions (DIET). In recent years, technological progress has made it possible to perform time-resolved laser pump–probe experiments in which the time evolution of DIET processes can be monitored in the femtosecond regime [2]. These experiments provide a wealth of information on the real-time dynamics of chemical processes at surfaces (see, for example, [3, 4]).

Unfortunately, the experimental progress has not been accompanied by a corresponding development of theoretical tools for the realistic description of DIET processes. This is mainly due to the fact that the modeling of processes involving electronic transitions still represents a great challenge. First of all, the ab initio determination of excited state potentials is not possible using computational efficient density-functional theory schemes. One has to use quantum chemistry methods, which are usually computationally very costly. Secondly, the simulation of the dynamics of DIET processes requires the explicit treatment of both electronic and nuclear dynamics. There has been significant progress in the high-dimensional simulation of Born–Oppenheimer reaction dynamics at surfaces in recent years [5–7]. These studies have demonstrated the importance of multi-dimensionality in the reaction dynamics. However, electronically non-adiabatic simulations of reactions at surfaces are usually limited to a few degrees of freedom [8]. This is caused by difficulties in the theoretical treatment resulting from the different time scales in the electronic and nuclear motion.

In order to allow a multi-dimensional treatment of laser-induced desorption, we propose the use of a mixed quantum-classical scheme in which the nuclear motion is described classically while the electrons are treated quantum mechanically. The feedback between quantum and classical degrees of freedom still has to be taken into account self-consistently. We have recently implemented such a scheme for the description of charge transfer processes in the scattering of molecules at surfaces [9, 10]. This mixed quantum–classical scheme is based on the fewest switches algorithm developed by Tully [11]. In this surface-hopping algorithm, the number of state switches is minimized under the constraint of maintaining the correct statistical population of each state.

We have now extended this algorithm in order to address laser-induced reactions at surfaces. Combining ideas of previous treatments [11–14], we have in particular introduced an optical potential in order to simulate the collective influence of electronic excitations of the substrate. Our mixed quantum–classical (MQC) method allows the inclusion of the relevant nuclear coordinates of both adsorbates and the substrate at sufficiently long propagation times to correctly describe thermalization and dissipation effects. In order to establish the validity of our scheme, we first compare the results of our method to two-dimensional jumping wave-packet calculations [15] of the laser-induced desorption of NO from

✉ Fax: +49-89/289-12296, E-mail: axel_gross@ph.tum.de

NiO(100) using exactly the same potential energy surface (PES), which was derived from ab initio calculations [16].

This system has been well studied experimentally [17–20]. One of the most interesting experimental results is the bimodality that has been observed in the velocity distribution of desorbing molecules [17]. Based on the wave-packet calculations, it was proposed that the bimodality is a consequence of a bifurcation of the wave-packet due to the topology of the excited state potential energy surface [15].

In order to study the influence of additional degrees of freedom on the desorption process, we extended the potential energy surface to seven dimensions in total by considering the remaining NO degrees of freedom and one surface oscillator coordinate. In the absence of any ab initio calculations we used a physically reasonable model potential for this extension. Indeed, the incorporation of the higher dimensionality, in particular the recoil effects at the surface, turn out to strongly modify the desorption dynamics. The bimodality in the velocity distribution, observed in a low-dimensional description and in the experiment, disappears in a high-dimensional treatment. These findings demonstrate the importance of a realistic multi-dimensional treatment of the desorption dynamics. It also indicates that further studies have to be performed in order to fully understand the laser-induced desorption of NO from NiO(100)

This paper is structured as follows. After this introduction, we first lay out our proposed mixed quantum–classical scheme for the description of laser-induced desorption processes at surfaces. Then we address the construction of the high-dimensional potential energy surface. The results of our calculations are discussed in detail, and then the paper ends with some concluding remarks.

A brief account of this work has appeared elsewhere [21]. In this paper, the theoretical method is described in more detail. Furthermore, we report additional results of the mixed quantum–classical calculations with respect to the kinetic energy distribution and the vibrational distribution in desorption.

2 Theory

2.1 *Model*

DIET processes are usually described within the Menzel–Gomer–Redhead (MGR) model [22, 23] or the Antoniewicz model [24], which differ in the relative position of the minima in the ground and excited state potentials. Still, both models assume the same reaction steps, which are illustrated in Fig. 1. First the system is excited by, for example, a laser pulse. This pulse may directly excite the adsorbate, but most probably, the substrate first becomes electronically excited with the creation of hot electrons (step 1). The adsorbate then becomes electronically excited in a Franck–Condon transition, for example, by the transfer of one electron from the substrate (step 2). Such a mechanism has been proposed for the laser-induced desorption of NO from NiO [17], but direct excitations have also been suggested [25]. Since the minimum energy positions of the ground and excited states differ in general, the adsorbate in the excited state becomes accelerated (step 3). After a certain period of time, the adsorbate returns to the electronic ground state with the excess energy being transferred to the substrate (step 4). Depending on how much kinetic energy the adsorbate gains in this process, it may desorb (step 5) or not.

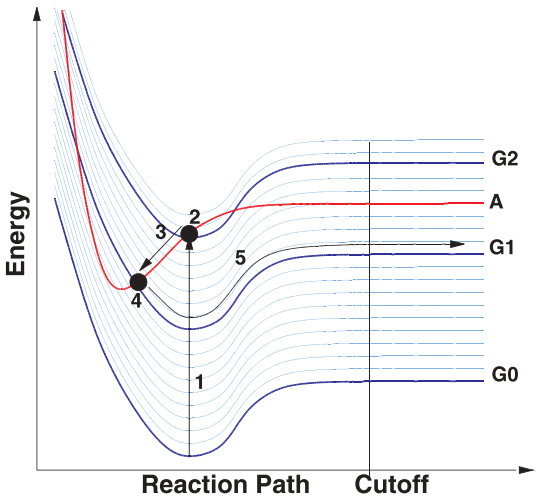

FIGURE 1 Schematic drawing of a DIET process. The potential curves labeled G0–G2 correspond to the adsorbate ground state with different substrate excitations, while the curve labeled A corresponds to an excitation of the adsorbate. *Thin dashed lines* represent the adsorbate ground state together with substrate states that are not explicitly involved. The numbers 1–5 indicate the five steps of the desorption process

In fact the adsorbate may become electronically excited more than once. This would correspond to a DIMET process: desorption induced by multiple electronic excitations. As far as NO/NiO is concerned, however, the linear dependence of the desorption yield on the laser fluence [20] leads to the exclusion of multiple excitations.

One of the problems encountered when modeling such processes is the huge number of electronic substrate states involved, which have to be treated quantum mechanically. It is clear that it is neither feasible nor necessary to explicitly include all these substrate states in our simulation. The reaction dynamics is dominated by a few adsorbate states, which have to be taken into account. But the main effect of the substrate states of coupling different adsorbate states either to each other or to an external electromagnetic field can be treated collectively. To model this effect we combine ideas from Tully's fewest switches algorithm [11] and the generalized surface hopping method [12] with those of Brenig [13] and Saalfrank [14], who introduced optical potentials into the description of DIET processes. First we separate the nuclear from the electronic degrees of freedom, that is, the Hamilton operator H is split into the kinetic energy T_R of the nuclear coordinates R and an electronic part H_e depending explicitly on the electronic coordinates r and parametrically on the position of the nuclei R:

$$H(r, R) = T_R + H_\mathrm{e}(r, R)\,. \tag{1}$$

The electronic wave function Φ is expanded into the explicitly treated excited adsorbate states φ_i and a collective state ψ containing the molecular ground state together with the continuum of substrate excitations:

$$\Phi(r, R, t) = \sum_i c_i(t)\varphi_i(r, R) + \psi(r, R, t)\,.$$

The influence of the collective state ψ can be taken into account by an effective non-Hermitian Hamiltonian (see Chapter 16 in [26]),

$$H_{\text{eff}}(r, R) = T_{\text{e}} + V_{\text{eff}}(r, R) + i\Delta(r, R)\,, \tag{2}$$

where T_{e} is the kinetic energy operator for the electrons. The effective potential V_{eff} and the optical potential Δ are real functions of r and R. In a Newns–Andersson [27] picture, Δ is related to the lifetime broadening of a resonance state, which can be determined via

$$\Delta(E) \;=\; \pi \sum_{\boldsymbol{k}} |V_{\boldsymbol{k}}|^2 \delta(E - \varepsilon_{\boldsymbol{k}})\,. \tag{3}$$

With the effective Hamiltonian and a diabatic (i.e. $\nabla_R \varphi_i = 0$) representation of the wave functions φ_i, the electronic Schrödinger equation has the following form:

$$\dot{c}_j = -\frac{i}{\hbar} \sum_i c_i V_{ji} + \frac{1}{\hbar} \sum_i c_i \Delta_{ji}\,, \tag{4}$$

where the matrix elements V_{ij} and Δ_{ji} are defined as

$$\begin{aligned} V_{ji} &\equiv \left\langle \varphi_j \middle| T_{\text{e}} + V_{\text{eff}}(r, R) \middle| \varphi_i \right\rangle\,, \\ \Delta_{ji} &\equiv \left\langle \varphi_j \middle| \Delta(r, R) \middle| \varphi_i \right\rangle\,, \end{aligned} \tag{5}$$

respectively. For the diagonal elements of the density matrix $a_{ji} \equiv c_j^\star c_i$, this leads to

$$\dot{a}_{jj} = \sum_i b_{ji} + \sum_i \frac{2}{\hbar} \operatorname{Re}\left[a_{ji}\Delta_{ji}\right]\,, \tag{6}$$

with $b_{ji} \equiv \frac{2}{\hbar} \operatorname{Im}\left[a_{ji} V_{ji}\right]$. Note that for a normalized wave function Φ the occupation probability a_{cc} for the "rest" is simply given by $a_{\text{cc}} \equiv 1 - \sum_j a_{jj}$, leading to

$$\dot{a}_{\text{cc}} = -\sum_j \dot{a}_{jj} = -\frac{2}{\hbar} \sum_{ij} \operatorname{Re}\left[a_{ji}\Delta_{ji}\right]\,, \tag{7}$$

since $\sum_{ji} b_{ji} = 0$. The nuclear coordinates R are treated classically and obey the Newtonian equation of motion

$$\ddot{R} = \frac{-1}{M} \nabla \left[\frac{\langle \psi_{\text{occ}} | H_{\text{e}} | \psi_{\text{occ}} \rangle}{\langle \psi_{\text{occ}} | \psi_{\text{occ}} \rangle} \right]\,, \tag{8}$$

where ψ_{occ} is the currently occupied state. Both the classical and quantum dynamics are determined self-consistently. This means that the particular PES on which the atoms move in a classical fashion depends on the electronic expansion coefficients c_j. These coefficients, on the other hand, are determined by integrating the time-dependent Schrödinger equation with a Hamiltonian that is time-dependent via the atomic coordinates. The probability for the hops between the different potentials $\langle \psi_{\text{occ}} | H_{\text{e}} | \psi_{\text{occ}} \rangle$ / $\langle \psi_{\text{occ}} | \psi_{\text{occ}} \rangle$ for the classical motion are chosen according to the fewest-switches algorithm [11], which has also been used in the generalized surface hopping method [12]. In this algorithm, the probabilities of jumping to a particular state are constructed in such a way that for a swarm of trajectories the probability of finding a trajectory in state j is the same as $P_j(t) = a_{jj}$. This is achieved in the following way: (4) and (8) are integrated numerically over a certain time step Δt. After each integration step, it is decided whether to jump to a different PES or not. This is done by comparing the probability of going from state j to state i,

$$p_{ji} = \frac{\Delta t\, 2 \operatorname{Im}(a_{ij} V_{ij})}{\hbar a_{jj}}\,, \tag{9}$$

and the probability of going from k to the collective state ψ,

$$p_{jc} = \frac{-2\Delta t}{\hbar a_{jj}} \sum_i a_{ji} \Delta_{ji}\,, \tag{10}$$

with a uniformly distributed random number between 0 and 1. In principle, the switches between the states can occur at any point along the trajectories. Note that switches into the collective state occur only if the sum $\sum_i a_{ji}\Delta_{ji}$ is negative. This formalism can also be used to describe the excitation from the collective state into a particular electronic state j. For such a transition the sum has to be positive, that is, the sign of the optical potential basically has to be reversed.

Our approach differs to a certain extent from the generalized surface hopping method [12]. First, we have introduced an optical potential in order to describe transitions to the collective state ψ. Furthermore, in our scenario we assume that all of the excess energy upon a transition to the continuum state is taken up by the substrate electrons, as is usually done in the modeling of laser-induced desorption [8]. This means that upon a switch to the continuum state, we just make a Franck–Condon transition; that is, we transfer the molecule to the ground state potential with its kinetic energy preserved and perform ordinary Born–Oppenheimer molecular dynamics until the final fate of the molecule has been determined.

If just one electronically excited state is considered, then the equations become much simpler. According to (6) and (7), the de-excitation rate is directly given by

$$\dot{a}_{11} \;=\; -\dot{a}_{\text{cc}} \;=\; \dot{c}_1 c_1^* + c_1 \dot{c}_1^* = \frac{2a_{11}\Delta}{\hbar}\,. \tag{11}$$

In fact, for such a situation no electronic Schrödinger equation has to be integrated.

Our method could in principle also be extended to include the excitation process. Furthermore, taking the explicit time dependence into account is also straightforward. This could be used, for example, to model the pulse shape of the exciting laser or the thermalization of hot electrons in the case of an indirect process.

2.2 *Procedure*

We start our trajectories in the excited state, where they move classically for a certain time. After a Franck–Condon transition the movement of the molecule is continued on the ground state potential for a maximal propagation time or until it reaches a certain distance Z_{Cutoff} from the surface and is considered desorbed.

The trajectories are started around the position of the ground state minimum, assuming a Gaussian distribution in position and momentum according to the curvature of the

ground state potential energy surface. This corresponds to a harmonic approximation for the potential at the minimum position. In principle, the distributions should be given by the true ground state wave function, but since the masses of the nuclei are rather large and the anharmonicity of the potential is small, this is a good approximation.

After each integration step in the excited state, we decide whether to continue in the excited or the ground state by comparing the decay probability $p = 2\Delta(R)\mathrm{d}t/\hbar$ with a random number between 0 and 1.

For a constant Δ, this procedure is equivalent to the Gadzuk scheme [28] as used in [15]. In this scheme the lifetime of the molecules in the excited state, the so-called residence time, is kept fixed in a simulation run. The overall result is obtained by averaging over several simulation runs with different residence times t with a weight function $w_\tau(t) = \tau^{-1}\exp(-t/\tau)$, where the average residence time or resonance lifetime τ is an adjustable parameter. It can be directly connected to the strength of the optical potential via

$$\tau = \frac{\hbar}{2\Delta} . \tag{12}$$

2.3 *Potentials*

The potential energy surfaces we used in our simulation are based on two two-dimensional potentials V_{ai} from Klüner et al. [29], one representing the electronic ground state and the other a charge transfer state in which an electron from the substrate is transferred to an adsorbate state. These potentials were obtained by fitting analytical expressions to energies from ab initio calculations. The two degrees of freedom used are the molecule–surface distance Z and the polar angle θ.

In order to come to a complete description of the NO molecule, we extended the ab initio two-dimensional potentials to six dimensions. In the absence of any ab initio results, we were required to use a model potential for the additional degrees of freedom. Thus the particular choice of the parameters has to be considered an educated guess. We would like to point out, however, that the qualitative results we obtained did not depend very sensitively on the particular choice of parameters. The potential energy surface is

$$V^s_{6\mathrm{D}}(X, Y, Z, r, \theta, \varphi) = V^s_{ai}(Z, \theta) + V_{\mathrm{cor}}(X, Y, Z) + V_{az}(X, Y, Z, \theta, \varphi) + V^s_{\mathrm{NO}}(r) . \tag{13}$$

The upper index s is either g or e, denoting the ground or the excited state. For potentials for which this index is absent, we do not distinguish between the two states. The X and Y coordinates give the lateral position on the surface, φ is the azimuthal angle, and r is the N–O distance in the NO molecule. The corrugation potential V_{cor} is given by

$$V_{\mathrm{cor}}(X, Y, Z) = \frac{C_{\mathrm{cor}}}{4}\mathrm{e}^{-\lambda_{\mathrm{cor}}(Z-Z_0)}\,(2 - \cos G_X X - \cos G_Y Y) , \tag{14}$$

and the azimuthal dependence is

$$V_{az}(X, Y, Z, \theta, \varphi) = \frac{C_{az}}{2}\mathrm{e}^{-\lambda_{az}(Z-Z_0)}\cos 2\varphi \sin\theta\,(\cos G_X X - \cos G_Y Y) . \tag{15}$$

This corresponds to a molecule with two equal atoms, but as a first approximation, it suffices. The strength of the corrugation was set to $C_{\mathrm{cor}} = 1.0\,\mathrm{eV}$ and that of the azimuthal dependence to $C_{az} = 0.25\,\mathrm{eV}$, with decay lengths of $\lambda_{\mathrm{cor}} = \lambda_{az} = \frac{1}{2}\,\mathrm{Å}^{-1}$. The lattice constants G_X and G_Y were set to the Ni–Ni distance of the NiO(100) surface, $G_X = G_Y = 2.942\,\mathrm{Å}$, as used in [29]. The NO potential is given by a Morse potential with different parameters for the ground and the excited state:

$$V^s_{\mathrm{NO}}(r) = C^s_{\mathrm{NO}}\left(1 - \mathrm{e}^{-\alpha_s(r-r_s)}\right)^2 . \tag{16}$$

The parameters used for the N–O potential were $C^{\mathrm{g}}_{\mathrm{NO}} = 6.5\,\mathrm{eV}$, $\alpha_{\mathrm{g}} = 1.68\,\mathrm{Å}^{-1}$, and $r_{\mathrm{g}} = 2.175\ \mathrm{a_0} = 1.151\,\mathrm{Å}$ in the ground state, and $C^{\mathrm{e}}_{\mathrm{NO}} = 4.5\,\mathrm{eV}$, $\alpha_{\mathrm{g}} = 1.50\,\mathrm{Å}^{-1}$, and $r_{\mathrm{g}} = 2.225\ \mathrm{a_0} = 1.177\,\mathrm{Å}$ in the excited state, in accordance with [30].

In order to model recoil effects of the substrate, we included a surface oscillator with coordinate s by directly coupling a harmonic potential to the desorption coordinate, which in our case is the distance from the surface Z:

$$V^s_{\mathrm{N+osc}}(s, Z, R) = V^s_{\mathrm{N}}(Z - s, R) + V_{\mathrm{osc}}(s) , \tag{17}$$

where R denotes all other coordinates. The mass of the oscillator was taken to be equal to the mass of a Ni atom (58 amu), since NO is adsorbed on top of a Ni atom. The oscillator frequency was chosen to correspond to the average value of a Debye spectrum, as is usually done in simulations using the surface oscillator model [31]. The Debye temperature of NiO was estimated to be between 500 and 600 K [32]. Accordingly, we set the oscillator frequency to $\hbar\omega = 27\,\mathrm{meV}$. In any case, the effect of the surface oscillator on the desorption dynamics is not very sensitive to the particular choice of the frequency. In the following section, we report results of 2D and 6D simulations without and with the surface oscillator, denoted by 2D, 3D, 6D, and 7D calculations, respectively.

3 Results and discussion

In order to validate the classical treatment of the nuclear coordinates we first tried to reproduce the wave-packet results of Klüner et al. [15] by performing equivalent two-dimensional molecular dynamics simulations using the same ab initio potential energy surface and the Gadzuk scheme with a resonance lifetime of 24.19 fs (= 1000 a.u.). In agreement with the wave-packet calculations, we only found appreciable desorption probabilities for molecules that stayed on the excited state potential for more than 50 fs. However, the wave-packet calculations gave a total desorption yield of 3.3%, whereas the classical simulations lead to 4.8%. This was puzzling as we expected the wave-packet results to give a higher yield due to desorption from classically forbidden tails of the wave function. Closer examination of the desorption probability as a function of time helped to resolve this

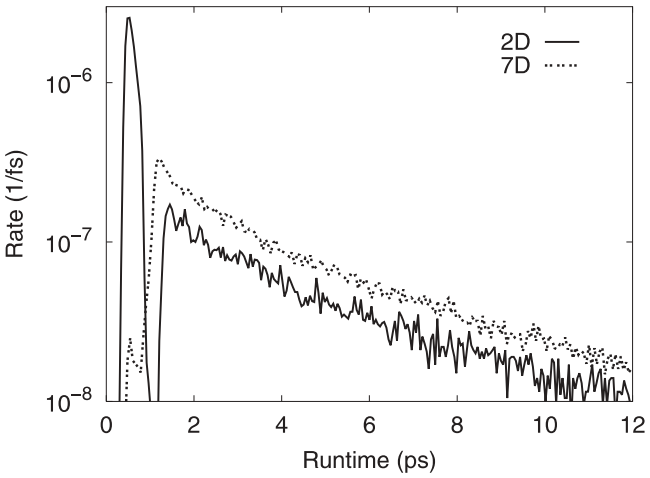

FIGURE 2 Desorption rate as a function of time (excitation at time $t = 0$) in the 2D (*solid line*) and 7D simulations (*dash-dotted line*). The 2D results were obtained with a cutoff distance of $Z_{\mathrm{Cutoff}} = 12.5$ a.u., while in the 7D calculations $Z_{\mathrm{Cutoff}} = 16.0$ a.u. was chosen

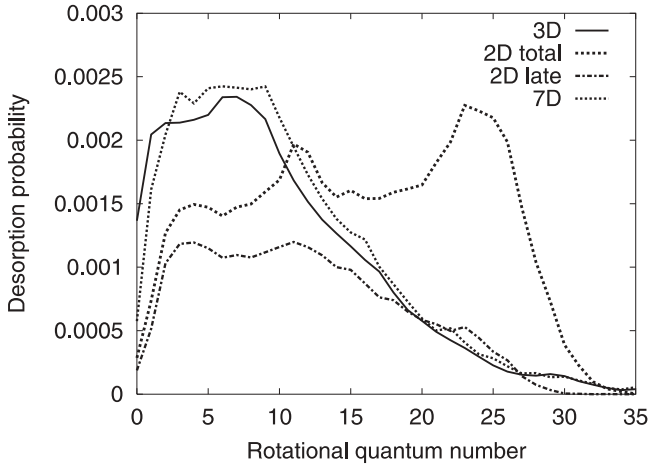

FIGURE 3 Comparison of the rotational momentum distributions with (3D and 7D simulations) and without (2D simulations) the surface oscillator

discrepancy. As can be seen in Fig. 2, there are two kinds of desorbing trajectories, early (within the first 1.2 ps) and late ones. The wave-packet results were obtained by propagating in the ground state until the desorption yield saturated after 1.2 ps. Note that for the 2D results there is a gap in the desorption probability at that time. When we consider only the early desorbing trajectories, the desorption probability goes down to 2.91%, in much better agreement with the wave-packet results. For better comparison with the wave-packet simulations a cutoff distance of $12.5a_0$ was chosen. When going to larger cutoff distances, the early desorption probability naturally goes down (2.49% for $16.0a_0$ and 1.56% for $20.0a_0$) and the gap in the desorption flux also vanishes. The total desorption probability does not depend on the cutoff distances. When not comparing with the wave-packet results we will use a cutoff distance of $16.0a_0$, since at $12.5a_0$ the binding energy is still 10 meV. Note that for our method the computational cost in increasing the cutoff distance is small compared with that in the wave packet case.

The phenomenon of the early and late desorbing molecules can be understood by closer examination of single trajectories and by taking the position of the potential energy surface minima into account. In the ground state minimum the NO molecule is tilted from the surface normal by 45°. In the excited state, the minimum is an upright position closer to the surface. Thus upon excitation the molecule is accelerated towards the surface and into an upright position. For the lifetimes we used, most molecules relax to the ground state before they reach the excited state minimum. On the ground state the molecules hit the repulsive potential wall and either scatter directly into the vacuum, giving the early desorbing species, or start to rotate in front of the surface and are trapped or desorb after one or more rotations, leading to the late species. The molecules scattered directly into the vacuum have high translational and rotational momentum. The difference in the rotational momentum distribution between the late and early trajectories can be seen in Fig. 3, in which we plot the distributions for all and the late trajectories only. The late molecules show a broad peak between $J = 3$ and 11 and fall off for higher momenta. The early species shows a large peak at $J = 25$ and a smaller one at $J = 12$ (see Fig. 4). Note that for a freely rotating NO molecule, the rotational period T is connected to the rotational quantum number J and the moment of inertia I via $T = (2\pi I/\hbar)/J$, where $2\pi I/\hbar$ is equal to 9.79 ps for NO. Thermalization would eventually lead to the suppression of the late desorption, but on a much larger time scale of several picoseconds (the total time scale of our simulation is only 12 ps).

There is good qualitative agreement between the velocity distributions of the early desorbing classical trajectories and the wave-packet results from [15]. However, when also considering the late trajectories, the shape of the momentum distribution changes considerably and the agreement only remains for the highest rotational states. We also compared the Gadzuk scheme for relaxation into the ground state with decay using either a constant or an exponentially decreasing optical potential. The mean lifetime τ and the strength of the optical potential Δ_0 are related via

$$\Delta_0 = \frac{\hbar}{2\tau}\,, \tag{18}$$

and the spatial dependence of optical potential is given by

$$V_{\mathrm{opt}} = V_{\mathrm{opt}}(Z) = \Delta_0\, \mathrm{e}^{-\gamma(Z-Z_0)}\,, \tag{19}$$

where Z_0 is the ground state equilibrium distance of the NO molecule from the surface. A zero inverse decay length γ corresponds to a constant V_{opt}. The use of an exponentially decaying optical potential is motivated by the fact that the coupling between the ground and the charge transfer state is given by the overlap of the molecular state with the bulk electrons. As expected we found no significant difference between the constant optical potential and the Gadzuk scheme, neither for the desorption probability nor for the momentum distributions. More surprising was that switching on the exponential decrease of the optical potential had basically no effect on the velocity distributions and only changed the total desorption probability.

In our high-dimensional treatment, we also analyzed the vibrational population of desorbing molecules. When extending the two-dimensional ab initio potential energy surface to

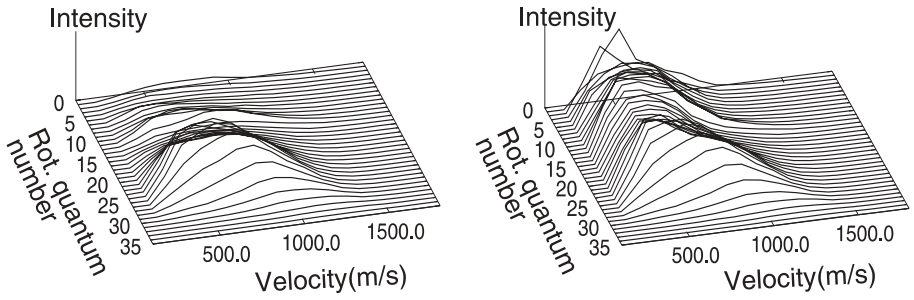

FIGURE 4 Velocity distributions for early (*left*) and all (*right*) desorbing molecules in the two-dimensional MQC simulation

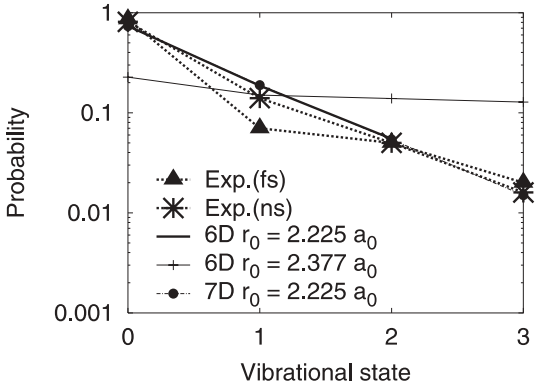

FIGURE 5 The vibrational excitation for different models. The experimental values were taken from [18]

six dimensions, we first used the gas phase value of $r_{NO} = 2.377a_0 = 1.258$ Å for the NO^- ion equilibrium distance. As is well known [1, 30], this leads to unrealistically high vibrational excitations, because of the large displacement in the vibrational coordinate in the NO^- state. This behavior is reproduced in our calculations (see Fig. 5, thin solid line). The relative vibrational populations P_v/P_0 of the vibrationally excited states characterized by the vibrational quantum number v are much larger than the ones derived from the experiment.

However, the strong electrostatic field above the ionized NiO(100) surface reduces the N–O bond elongation of the NO^- anion according to quantum chemical calculations [30]. The anion bond is only extended by $0.05a_0 = 0.026$ Å compared with the neutral NO molecule above the NiO(100) surface instead of $0.2a_0$ as in the gas phase. Consequently, we used a N–O bond distance of $r_g = 2.225a_0 = 1.177$ Å for the NO^- anion in the excited state. In accordance with [30] we get good agreement with the experimental values of the vibrational population of desorbing NO molecules.

Furthermore, we observed that the total desorption probability did not change within the level of the accuracy of our simulations when we varied the NO^- equilibrium distance. This indicates that energy transfer from the vibrational coordinate into other degrees of freedom is very small, since when using the gas phase value for the N–O distance, half of the trajectories have enough energy to overcome the desorption barrier, but only 4.97% actually desorb within reasonable time. Not only does the desorption probability hardly change with r_{NO^-}, but the momentum and rotational momentum distributions also do not vary.

Since the mass of the substrate atoms and the NO molecule is comparable, recoil processes during the desorption process are probable. In order to include energy transfer to the substrate in the simulations, we have coupled the 2D and 6D potentials to a surface oscillator with realistic parameters, as described in the previous section. The computational costs of this extension are rather small.

In Table 1 we collect the main results with respect to the desorption probability and the rotational temperature of desorbing molecules according to the 2D, 3D, 6D, and 7D calculations. Going from 2D to 6D, that is, including the remaining molecular degrees of freedom in the simulations, has little influence on the desorption dynamics. The same is also true for the transition from 3D to 7D.

However, taking recoil processes of the substrate into account by including a surface oscillator changes the outcome of the trajectory calculations significantly. While the total desorption probability is only reduced by about 1%, the effect on the early desorption channel is very dramatic: it is reduced by a factor of eight. This can also be seen in the desorption rate in Fig. 2, in which the initial "early" peak is basically absent in the 7D results. This also affects the rotational momentum distribution. While in the 2D calculations we obtained a double peaked structure with a large probability for high rotational quantum numbers j, the inclusion of the surface oscillator causes the suppression of the peak at high j. The distribution is similar to that of the late molecules in the rigid surface case. This results in a greatly reduced mean rotational energy in desorption, 366 and 395 K for the 3D and 7D calculations, respectively, instead of 770 and 883 K for the 2D and 6D calculations, respectively. These reduced rotational temperatures are in fact in much better agreement with experiment [17]. As far as the vibrational population in desorption is concerned, Fig. 5 demonstrates that it is hardly influenced by going from six to seven dimensions. This indicates that the vibrational dynamics is efficiently decoupled from the remaining degrees of freedoms due to the fact that it corresponds to the shortest time scale in the molecular dynamics.

As far as the comparison between experiment and theory with respect to the velocity distribution is concerned, how-

	2D	3D	6D	7D
z_{CO} (a_0)	12.5	16.0	16.0	16.0
P_{des} (%)	4.84	3.63	4.74	4.02
P_{early} (%)	2.93	0.32	2.53	0.32
E_{rot} (K)	770	366	883	395

TABLE 1 Desorption probabilities and mean rotational energies according to the 2D, 3D, 6D, and 7D calculations Early means desorption within the first 1.2 picoseconds

ever, the agreement is greatly reduced if the late desorption channel and the surface oscillator are taken into account. In Fig. 6, we plot the velocity distribution according to the 7D calculations. The velocity distribution for the 3D simulation is rather similar, whereas the 6D results compare well to the 2D distribution, as shown in Fig. 4. There is no indication of the bimodal velocity distribution that was found in the experiment [17] and which was also reproduced in the wave-packet calculations [15]. Note that apart from an overall scaling due to the reduced desorption probability, the shapes of the velocity distributions summed over all rotational momenta are almost identical for all dimensionalities used.

Our high-dimensional simulations demonstrate the importance of multi-dimensionality in the reaction dynamics. Unfortunately, the agreement between theory and experiment becomes worse, in particular due to the inclusion of surface recoil effects. These findings do not necessarily imply that the conclusions of [15] with respect to the origins of the bimodality in the velocity distribution are no longer valid. In [15] it was proposed that the bimodality is a consequence of a bifurcation of the wave-packet due to the topology of the excited state potential energy surface.

On the basis of our calculations we cannot offer a novel explanation for the bimodality. We deliberately did not try to play around too much with the parameters of the potential in order to keep the ab initio character of the PES in the Z and θ coordinate. It might well be that the explanation given in [15] is still correct. However, in the simulations, only one excited charge transfer state potential out of a great number of charge transfer states [29] was chosen. It is possible that more than one excited state may be involved in the desorption process. Furthermore, the extension of the two-dimensional ab initio potential to seven dimensions using a physically reasonable model potential may not be realistic enough. This will be checked by mapping out high dimensional potential energy surfaces through quantum chemical calculations. Finally, the consideration of a more complex spatially varying transition probability could lead to better agreement between theory and experiment. If the de-excitation mainly occurs at specific configurations of the adsorbate, this can have a strong effect on the desorption dynamics. From a computational point of view, the simulation of such processes within our mixed quantum-classical scheme is indeed feasible and will be addressed in the future.

As mentioned above, our mixed quantum–classical scheme can also be used to describe excitation processes. We have performed initial preliminary calculations simulating time-correlated two-pulse laser-desorption experiments of NO from NiO(100) [19]. In these experiments, correlation times of 5–8 ps were found, depending on the vibrational state. Surprisingly, for the vibrational ground state a decrease in the desorption signal was found in the correlation experiments, while the higher vibrational states showed an increase. We modeled these experiments by describing the excitation due to the second laser pulse with a positive time-dependent optical potential. Our first calculations showed that our mixed quantum classical scheme allows sufficiently long propagation times to address the large time delays used in the experiment. However, more refined calculations have to be performed before the obtained correlations can be analyzed in detail.

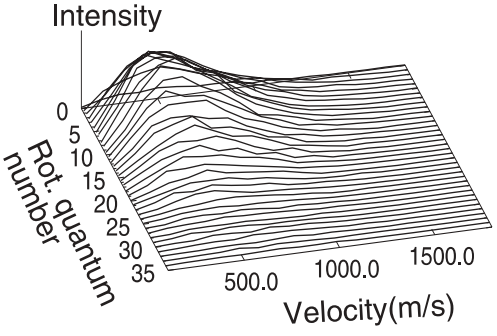

FIGURE 6 Velocity distribution for the 7D MQC simulation

4 Conclusion

In this paper we have presented a mixed–quantum classical scheme for the description of laser-induced desorption processes in which the nuclear motion is treated classically while the electron dynamics is treated quantum mechanically. The main motivation for such a scheme is its computational efficiency, which allows a realistic high-dimensional treatment of the desorption dynamics. We first showed that our method is able to reproduce the results of lower dimensional jumping wave-packet calculations for the desorption on NO from NiO(100). This confirms that quantum effects are indeed negligible in the nuclear dynamics of molecules such as NO.

Furthermore, we have demonstrated that our method is suited to a high-dimensional treatment on a long time scale. We have simulated the laser-induced desorption using a seven-dimensional potential energy surface that includes all NO degrees of freedom and one surface oscillator coordinate. We found that the laser-induced desorption dynamics of NO/NiO(100) is rather complex, requiring long simulation times. The inclusion of the surface oscillator had a dramatic effect on the desorption dynamics, in particular on the rotational state distribution. In our high-dimensional treatment we were not able to reproduce the bimodality found in the experiment. We speculated that this result may be due to the fact that we only included one excited-state potential in the simulations or that the extension of the potential energy surface to seven dimensions using a model potential was not realistic enough. Alternatively, a realistic, spatially varying transition probability could improve the agreement with the experiment. Future research along this line is in progress.

REFERENCES

1 F.M. Zimmermann, W. Ho: Surf. Sci. Rep. **22**, 127 (1995)
2 M. Bonn, A.W. Kleyn, G.J. Kroes: Surf. Sci. **500**, 475 (2002)
3 M. Bonn, S. Funk, C. Hess, D.N. Denzler, C. Stampfl, M. Scheffler, M. Wolf, G. Ertl: Science **285**, 1042 (1999)
4 H. Petek, M.J. Weida, H. Nagano, S. Ogawa: Science **288**, 1402 (2000)
5 A. Groß: Surf. Sci. Rep. **32**, 291 (1998)
6 G.-J. Kroes: Prog. Surf. Sci. **60**, 1 (1999)
7 A. Groß: Surf. Sci. **500**, 347 (2002)
8 H. Guo, P. Saalfrank, T. Seidman: Prog. Surf. Sci. **62**, 239 (1999)
9 C. Bach, A. Groß: Faraday Discuss. **117**, 99 (2000)
10 C. Bach, A. Groß: J. Chem. Phys. **114**, 6396 (2001)
11 J.C. Tully: J. Chem. Phys. **93**, 1061 (1990)

12 D.S. Sholl, J.C. Tully: J. Chem. Phys. **109**, 7702 (1998)
13 W. Brenig: Z. Phys. B **23**, 361 (1976)
14 P. Saalfrank: Chem. Phys. **193**, 119 (1995)
15 T. Klüner, H.-J. Freund, V. Staemmler, R. Kosloff: Phys. Rev. Lett. **80**, 5208 (1998)
16 T. Klüner, H.-J. Freund, J. Freitag, V. Staemmler: J. Mol. Catal. A **119**, 155 (1997)
17 T. Mull, B. Baumeister, M. Menges, H.-J. Freund, D. Weide, C. Fischer, P. Andersen: J. Chem. Phys. **96**, 7108 (1992)
18 G. Eichhorn, M. Richter, K. Al-Shamery, H. Zacharias: Surf. Sci. **368**, 67 (1996)
19 G. Eichhorn, M. Richter, K. Al-Shamery, H. Zacharias: Chem. Phys. Lett. **289**, 367 (1998)
20 G. Eichhorn, M. Richter, K. Al-Shamery, H. Zacharias: J. Chem. Phys. **111**, 386 (1999)
21 C. Bach, T. Klüner, A. Groß: Chem. Phys. Lett. **376**, 424 (2003)
22 D. Menzel, R. Gomer: J. Chem. Phys. **41**, 3311 (1964)
23 P.A. Redhead: Can. J. Phys. **42**, 886 (1964)
24 P.R. Antoniewicz: Phys. Rev. B **21**, 3811 (1980)
25 H. Zacharias, G. Eichhorn, R. Schliesing, K. Al-Shamery: Appl. Phys. B **68**, 605 (1999)
26 R.G. Newton: *Scattering Theory of Waves and Particles* (McGraw-Hill, New York 1966)
27 R. Brako, D.M. Newns: Rep. Prog. Phys. **52**, 655 (1989)
28 J.W. Gadzuk: Surf. Sci. **342**, 345 (1995)
29 T. Klüner, H.-J. Freund, J. Freitag, V. Staemmler: J. Chem. Phys. **104**, 10030 (1996)
30 T. Klüner, S. Thiel, H.-J. Freund, V. Staemmler: Chem. Phys. Lett. **294**, 413 (1998)
31 A. Groß, W. Brenig: Surf. Sci. **302**, 403 (1994)
32 K.S. Upadhyaya, G.K. Upadhyaya, A.N. Pandey: J. Phys. Chem. Solids **63**, 127 (2002)